CHAPTER 86

A Fully Nonlinear 3D Method for the Computation of Wave Propagation

Andrew B. Kennedy[1] and John D. Fenton[1]

Introduction

The computational capabilities for calculating nonbreaking wave evolution have advanced a great deal in recent years. For fully nonlinear models, the adoption of multi-subdomain techniques (Wang et al., 1995, de Haas et al., 1996) has provided much greater efficiency while still allowing the calculation of wave transformation up to overturning. Still, computational times remain great enough that the application of these methods to three dimensional domains remains somewhat limited. The variable depth Boussinesq equations were originally developed with the twin assumptions of mild nonlinearity and frequency dispersion (Peregrine, 1967), but recently, beginning with Witting (1984), there have been concerted efforts to increase their range of applicability. Papers of particular note include Madsen and Sørensen (1992), Nwogu (1993), Wei et al. (1994), Schäffer and Madsen (1995), and Gobbi and Kirby (1996) (GK). Of these, all but GK assume a flow field that varies quadratically in the vertical coordinate y, while GK derive their equations for a quartic vertical variation in the velocity potential. All of these methods have at least one free parameter which is invariably used to calibrate model linear phase speed, linear shoaling, second order transfer functions, or some combination of the three, to known analytic results over a level bed or small slope. For these special conditions, the accuracy of the various Boussinesq equations may be greatly improved and, in fact, the above papers have shown that accuracy is also improved for conditions which differ significantly from the idealised situations used for tuning. However, it is not possible to place confidence in velocities, pressures, and higher order free surface nonlinearities calculated by any of these methods except in reasonably shallow depths. The one exception to this are the GK higher order Boussinesq equations, which are quite complex.

In Kennedy and Fenton (1995) a method was developed to calculate wave evolution over varying topography for one dimension in plan. The flow field was locally represented by a polynomial of arbitrary degree which analytically satisfied Laplace's

[1] Dept. of Mech. Eng., Monash University, Clayton, Vic. Australia 3168

equation. By applying continuity conditions between subdomains, an overall solution to the boundary value problem was obtained and highly accurate time stepping solutions could be obtained. A summary of this, plus another related method appears in Fenton and Kennedy (1996).

In this paper, a method is developed which uses some of the same ideas but is valid for three dimensional fluid motion (two dimensions in plan). Again, the velocity potential is represented in the vertical by a polynomial of arbitrary degree but here, a set of differential equations results for a local polynomial approximation (LPA) to the exact solution. This is shown to provide excellent linear and nonlinear results for a wide range of waves. The degree of polynomial may also be easily changed to give the level of accuracy desired for a particular problem.

Solution of Laplace's Equation

For nonbreaking wave motion, the flow field is usually represented by a velocity potential, $\phi(x,z,y,t)$, and fluid velocities are thus $(u,w,v) = (\partial\phi/\partial x, \partial\phi/\partial z, \partial\phi/\partial y)$, where x and z are the horizontal coordinates and y is the vertical coordinate. The continuity equation for fluid flow to be satisfied at every point in the domain then becomes

$$\frac{\partial^2\phi}{\partial x^2} + \frac{\partial^2\phi}{\partial y^2} + \frac{\partial^2\phi}{\partial z^2} = 0, \tag{1}$$

which is simply Laplace's equation in three dimensions. At any time t_0 this velocity potential is subject to the boundary conditions

$$\phi = \phi_s \quad \text{on } y = \eta, \tag{2}$$

and

$$\frac{\partial\phi}{\partial y} - \frac{\partial\phi}{\partial x}\frac{\partial h}{\partial x} - \frac{\partial\phi}{\partial z}\frac{\partial h}{\partial z} = 0 \quad \text{on } y = h, \tag{3}$$

where $h(x,z)$ is the bed elevation, and the free surface elevation $\eta\,(x,z,t)$ and velocity potential $\phi_s\,(x,z,t)$ are both known at time t_0. With the addition of appropriate conditions on the horizontal boundaries, these two conditions (2) and (3), along with the field equation (1) completely specify the problem and may be used to solve for the flow field.

The velocity potential function used here assumes a polynomial variation in the vertical coordinate such that

$$\phi\,(x,z,y,t) = \sum_{j=0}^{r} A_j\,(x,z,t)\,y^j, \tag{4}$$

where $r \geq 2$, and the A_j coefficients are independent and may vary in time.

From here, there are many directions that could be taken. The Boussinesq approach would be to create a Taylor series expansion about some point in the water column which satisfies the bottom boundary condition (3) to the order of accuracy desired, and proceed from there. However, it is desired here to use an approximation which

distributes error more evenly than is possible with a Taylor series, where error quickly increases away from the expansion point. The obvious approach would now be some sort of finite element method, but this would involve volume integrals, which are slow to compute. Furthermore, unless higher order elements were used, convergence would be slow, and introducing them would increase computational costs significantly.

Therefore, a different approach is used, which is simple in concept, and distributes the error in (1) over the water column. First, constraints are imposed so that the velocity potential satisfies (2) and (3). Next, the average and first $r-2$ weighted averages of (1) over the water column are set to zero, such that

$$\int_h^\eta y^l \left(\frac{\partial^2 \phi}{\partial x^2} + \frac{\partial^2 \phi}{\partial y^2} + \frac{\partial^2 \phi}{\partial z^2} \right) dy = 0, \quad l = 0, .., r-2. \tag{5}$$

The appropriate global horizontal boundary conditions finish the specification of the problem and a set of linear equations results, which may be solved as desired.

Once the flow field is known, the free surface elevations and velocity potentials may be updated in time using the evolution equations

$$\frac{\partial \eta}{\partial t} = \frac{\partial \phi}{\partial y} - \frac{\partial \eta}{\partial x}\frac{\partial \phi}{\partial x} - \frac{\partial \eta}{\partial z}\frac{\partial \phi}{\partial z} \quad \text{on } y = \eta, \tag{6}$$

and

$$\frac{\partial \phi_s}{\partial t} = C - g\eta - \frac{1}{2}\left(\frac{\partial \phi}{\partial x}^2 + \frac{\partial \phi}{\partial z}^2 + \frac{\partial \phi}{\partial y}^2 \right) + \frac{\partial \phi}{\partial y}\frac{\partial \eta}{\partial t} \quad \text{on } y = \eta. \tag{7}$$

Alternate Formulations for the Velocity Potential

It is possible to rearrange the form of the velocity potential given in (4) so that it has fewer parameters at each computational point. The velocity potential

$$\begin{aligned} \phi(x,z,y,t) \;=\; & \phi_s \left(\frac{y-h}{\eta - h} \right)^2 + A_B \left[(y-\eta) + \frac{f_2}{f_1}\frac{(y-\eta)(y-h)}{\eta - h} \right] \\ & + \frac{\partial A_B}{\partial x}\frac{\partial h}{\partial x}\frac{(y-\eta)(y-h)}{f_1} \\ & + \frac{\partial A_B}{\partial z}\frac{\partial h}{\partial z}\frac{(y-\eta)(y-h)}{f_1} + A_3 (y-h)^2 (y-\eta) \\ & + A_4 (y-h)^2 (y-\eta)^2 + \ldots \\ & + A_r (y-h)^2 (y-\eta)^{r-2}, \end{aligned} \tag{8}$$

where

$$f_1 = 1 + \frac{\partial h}{\partial x}^2 + \frac{\partial h}{\partial z}^2,$$

and

$$f_2 = 1 + \frac{\partial h}{\partial x}\frac{\partial \eta}{\partial x} + \frac{\partial h}{\partial z}\frac{\partial \eta}{\partial z},$$

analytically satisfies both (2) and (3). If made to satisfy (5), the resulting velocity potential will be identical to that described in the previous section. Furthermore, since

two fewer coefficients are defined at each point, computational speed should increase significantly. However, it is obvious that coding will be much more complex and, due to time constraints, and because the main thrust of this paper is to determine the accuracy of this LPA method, the velocity potential formulation of (8) was not used.

Linear Properties

Phase Speed

Using linearised versions of the free surface conditions (6) and (7), analytic LPA solutions for a given level of approximation, r, may be found for a plane progressive wave train. For the level of approximation $r = 2$ (y^2 terms included in ϕ), the phase velocity c is

$$\frac{c^2}{gd} = \frac{1}{1 + \frac{1}{3}(kd)^2}, \tag{9}$$

where g is the gravitational acceleration, d is the fluid depth, and k is the wavenumber. For the level of approximation $r = 3$ (y^3 terms in ϕ), the relationship is

$$\frac{c^2}{gd} = \frac{1 + \frac{1}{10}(kd)^2}{1 + \frac{13}{30}(kd)^2 + \frac{1}{80}(kd)^4}, \tag{10}$$

and using $r = 4$ (y^4 terms in ϕ), the phase velocity is

$$\frac{c^2}{gd} = \frac{1 + \frac{13}{105}(kd)^2 + \frac{1}{420}(kd)^4}{1 + \frac{16}{35}(kd)^2 + \frac{3}{140}(kd)^4 + \frac{1}{6300}(kd)^6}. \tag{11}$$

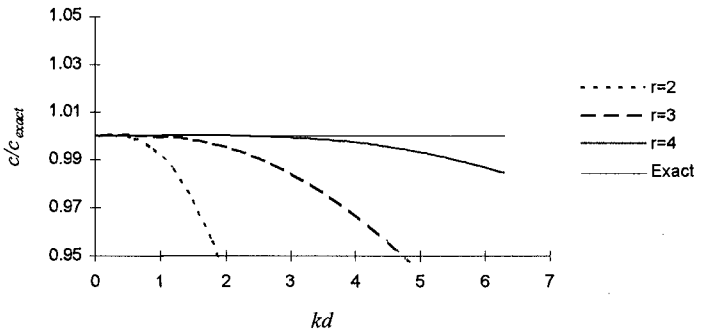

Figure 1. Small amplitude phase velocity

These expressions are identical to those obtained for Green-Naghdi shallow water Theories I, II, and III respectively (Shields and Webster, 1988). All of these are approximations to the exact small amplitude relationship

$$\frac{c^2_{exact}}{gd} = \frac{\tanh(kd)}{kd}. \tag{12}$$

In both (9) and (10) errors are of $O\left((kd)^4\right)$, while (11) contains errors of $O\left((kd)^8\right)$. Figure 1 compares LPA and exact phase speeds. Using the LPA level $r = 2$, phase speeds are found to be quite reasonable until a dimensionless wavenumber of $kd = 1.25$ $(L/d = 5)$ is reached, while with $r = 3$, phase speeds are adequate up until the nominal deep water limit of $kd = \pi$ $(L/d = 2)$. The level of approximation $r = 4$ gives very good results well into deep water and is usable even for a wave with $kd = 2\pi$ $(L/d = 1)$ which is a very pleasing result.

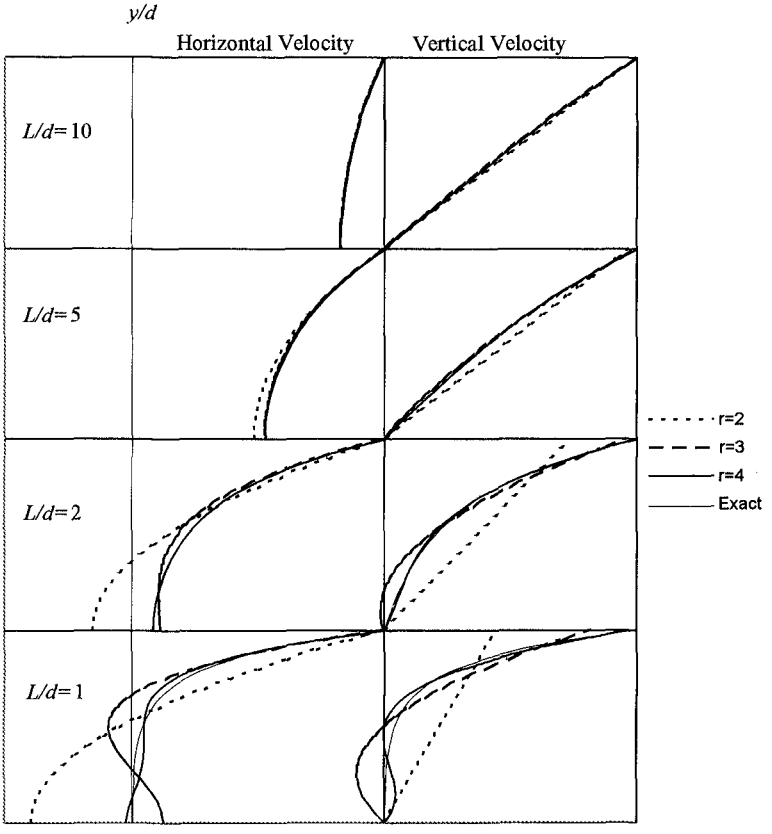

Figure 2. Normalised fluid velocities under a small amplitude wave

Fluid Velocities and Pressures

Small amplitude LPA solutions for ϕ may also be used to compare internal fluid velocities and pressures with Stokes first order results. Figure 2 shows the variation of the horizontal and vertical velocities, u and v, over the water column. For a wave with length $kd = \pi/5$ $(L/d = 10)$, all levels of LPA approximation give a good result,

although the level $r = 2$ shows slight differences, with the vertical velocity looking least accurate. Decreasing the wavelength to $kd = 2\pi/5$ ($L/d = 5$) increases error for the level $r = 2$, although all other levels predict velocities well. At the nominal deep water limit of $kd = \pi$ ($L/d = 2$), LPA levels $r = 2$ and $r = 3$ have significant errors in velocity, while with $r = 4$, the velocity is still modeled well. For a wave with length $kd = 2\pi$ ($L/d = 1$), all levels of approximation show error, although a convergence toward the exact solution is evident. Results for the dynamic pressure response factor $f(y)$, which gives the ratio of dynamic pressure at any elevation to the dynamic pressure just below the still water level, are identical to the results for relative horizontal velocity.

General Comments

With an overall view of the linear properties, some judgements may now be made. The first is that the level of LPA approximation $r = 2$ is only suitable for waves in shallow and mildly intermediate depths. For all other waves, the assumed structure of the velocity potential is inadequate to describe the vertical variation of the fluid flow. For these reasons, and since other levels are much more accurate, the level $r = 2$ will be discarded. The LPA level $r = 3$ gives significantly better results through to near the nominal deep water limit of $L/d = 2$, both for phase speed and fluid velocities. The level of approximation $r = 4$ has very accurate linear properties into quite deep water, and an increase to an LPA level to greater than this does not appear to be justified at the present time.

It is quite easy to introduce tuning parameters into the solution. By replacing (5) with the more general

$$\int_h^\eta w_l(y) \left(\frac{\partial^2 \phi}{\partial x^2} + \frac{\partial^2 \phi}{\partial y^2} + \frac{\partial^2 \phi}{\partial z^2} \right) dy = 0, \quad l = 0, .., r-2 \tag{13}$$

where $w_l(y)$ is some weighting function, sets $\{w_l\}$ were easily found which gave more accurate phase velocities for the LPA levels $r = 3, 4$. However, any increase in accuracy of phase velocity was invariably coupled with a decrease in accuracy of some other quantity of interest. For example, a set $\{w_l\}$ was found where the approximation of (11) for the LPA level $r = 4$ had errors decrease from $O((kd)^8)$ to $O((kd)^{10})$. However, errors in the horizontal velocity at the bed, which could be taken as another measure of accuracy, increased from $O((kd)^8)$ to $O((kd)^6)$. Because of results like this, and because the set of weighting functions $\{1, y, y^2, ...\}$ is very general, no attempt was made to tune the model for any particular quantity.

Nonlinear Properties

The nonlinear properties implied by the LPA set of governing equations were investigated by comparing their solutions for steady nonlinear waves with numerically exact solutions of the full potential flow equations. Numerically exact waves were generated using the Fourier method of Fenton (1988), while the fully nonlinear LPA solutions were found using the same general idea adapted to LPA.

Figure 3 compares LPA and numerically exact profiles for three highly nonlinear waves. The first wave generated is long, with a length to depth ratio of $L/d = 20$ ($kd = \pi/10$), and a height of $H/d = 0.6$. Both LPA levels $r = 3$ and $r = 4$ predict the profile very well. The second wave has length $L/d = 5$ ($kd = 2\pi/5$) and height $H/d = 0.4$. Once again, both LPA levels tested predict the nonlinear wave profile very accurately. The final wave in Figure 3 is at the nominal deep water limit, with a length to depth ratio of $L/d = 2$ ($kd = \pi$), and a height $H/d = 0.2$. For this wave, the LPA level of approximation $r = 3$ shows small errors, although the overall wave form is predicted well. However, the level $r = 4$ once again provides a solution which is indistinguishable by eye from the numerically exact profile.

Nonlinear phase speeds may also be compared with exact solutions. Figure 4 plots LPA and exact speeds for waves with length $L/d = 20$, 5, and 2. Circles, triangles and squares show the highest wave computed for the levels $r = 3$, $r = 4$, and numerically exact solutions, respectively. These do *not* represent the limiting waves, but instead describe a failure of the solution method to solve the system of nonlinear equations past these points.

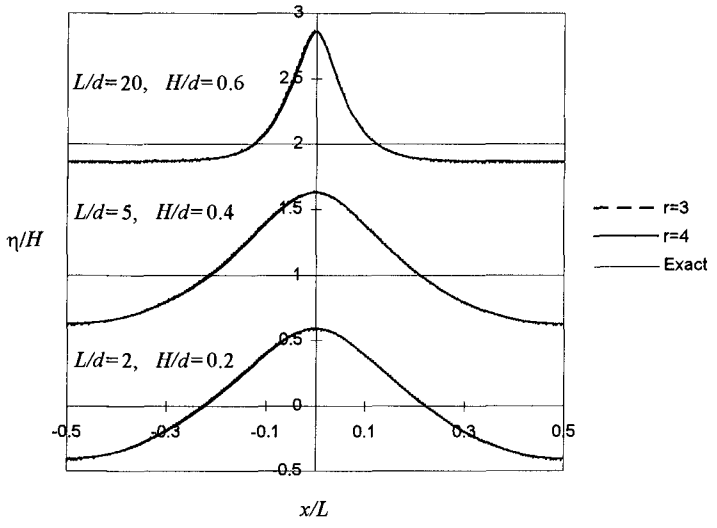

Figure 3. Nonlinear wave profiles

Both LPA levels $r = 3$ and $r = 4$ give a very good estimate of phase speed up to the highest waves tested, with the only significant differences occurring using $r = 3$ with a wave of length $L/d = 2$. However, even here the trend is followed quite well. The results for the level $r = 4$ and the wave with length $L/d = 5$ are especially noteworthy. Here, LPA solutions were found close to the limiting height which predicted the maximum and subsequent decrease in wave speed shown by

Cokelet (1977). This good representation of highly nonlinear waves gives additional confidence in the accuracy of the 3D LPA method.

Time Stepping Solutions

Time stepping solutions of the governing equations may be divided into two main tasks: the LPA solution of Laplace's equation, and the advance of the solution to the next time step. Of the two, the second is the most straightforward, as (6) and (7) were used with either a second order leapfrog or third order Adams-Bashforth technique to update the free surface elevations and velocity potentials. As neither of these methods are self starting, a fourth order Runge-Kutta technique was used for the first few time steps.

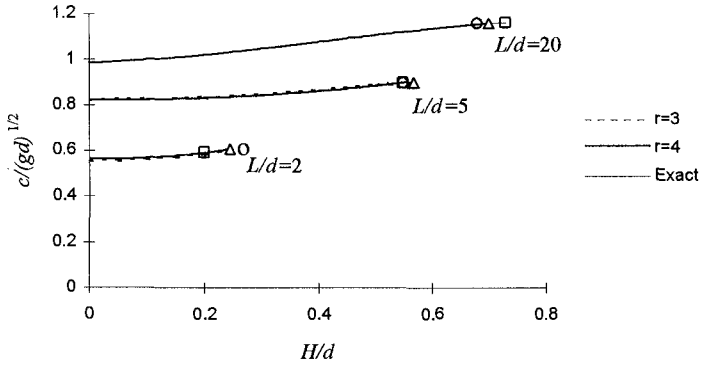

Figure 4. Nonlinear wave speeds

To solve Laplace's equation, all coefficients were represented using fifth degree two dimensional B-splines (see de Boor, 1978), which are simply the product of one dimensional B-splines in x and z which have the same centre. Solutions were also computed using third degree B-splines, but convergence was found to be poorer than desired. The sparse system of linear equations which results from the B-spline representation was solved using a line by line successive under-relaxation technique. Using this representation, errors in the LPA solution are theoretically proportional to $(\Delta l)^4$, where Δl is mesh size. This was tested by computing the maximum relative error in vertical velocity at the free surface for a flow field with a flat bed and surface, and free surface velocity potential $\phi_s = \cos(kx)$, where $kd = \pi/10$ $(L/d = 20)$. Figure 5 shows the relative error, plotted alongside $(L/\Delta l)^4$ for comparison. Convergence is seen to follow the theoretical behaviour closely. Furthermore, even for a very coarse representation of $\Delta l/L = 1/6$ (6 points/wavelength), relative errors are still only two parts in a thousand, which allows confidence to be placed in computations with relatively coarse resolution.

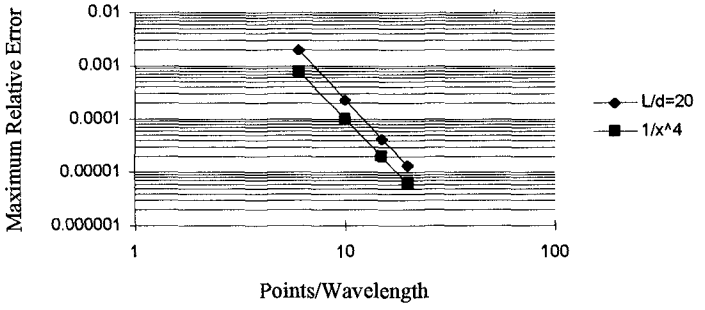

Figure 5. Convergence of the numerical scheme

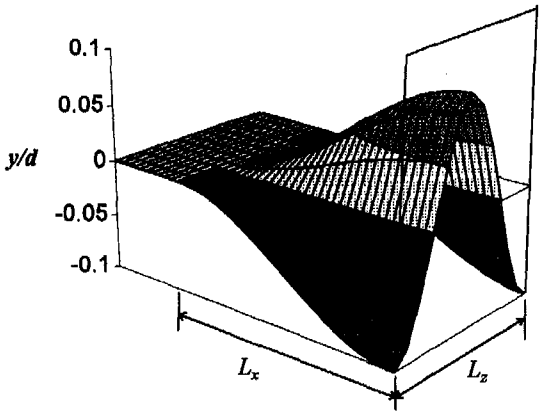

Figure 6. Bottom topography for solitary wave reflection

The Runup of a Focused Solitary Wave on a Vertical Wall

For a first test, a solitary wave of height $H/d = 0.2$ was propagated over topography which tended to focus the wave, which was then reflected by a vertical wall. Computations were performed using the LPA level $r = 4$. Figure 6 shows the focusing topography which consisted of a flat bed followed by a double cosine variation in the x and z directions with an amplitude of $0.1d$. However, for all x, the average bed elevation still remained $y = 0$. Different scales L_x and L_z as marked would focus the wave to different degrees, leading to a varying runup on the vertical wall. This numerical experiment could be thought of as representing the effect on solitary wave runup of small variations in topography about a mean. Figure 7 shows a snapshot of the wave's surface profile slightly after maximum runup. The three dimensional effects can clearly be seen.

Figure 8 shows the maximum runup of the wave for varying L_x and L_z. The computed

runup for a level bed and predicted runup for a wave propagated onto an infinite two dimensional shoal of depth $d_s/d_0 = 0.9$ are also shown. The latter result was predicted using the KdV results of Johnson (1973) and the solitary wave runup formula of Su and Mirie (1980). For small spatial scales, the topography has very little effect on runup but, as the scale increases, runup also increases significantly. Although the maximum value for the focused runup is only slightly greater than the predicted result for an infinite shoal, it is by no means clear that the limiting runup has been reached, and a further increase in L_x and L_z might well give significantly higher values.

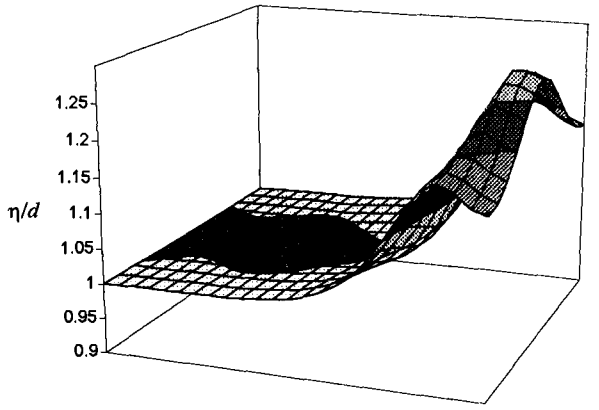

Figure 7. The reflection of a focused solitary wave by a vertical wall

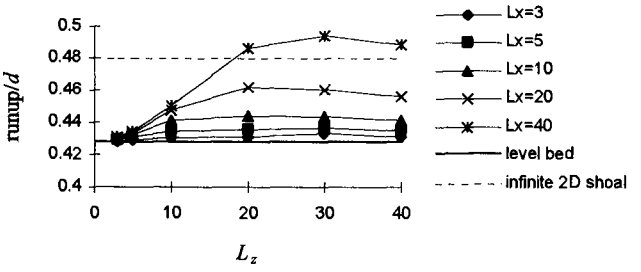

Figure 8. Maximum runup of a focused solitary wave

Since all of the above computations were performed in an enclosed space with no dissipation, conservation of energy could be used as an independent check on accuracy. For all tests, the maximum fluctuation in total energy at any point in time relative to the initial value was less than 2×10^{-4}.

The propagation of regular waves over Whalin's topography

For a final test of the LPA method, the propagation of regular waves over Whalin's

topography was computed. In a series of experiments, Whalin (1971) propagated waves over a semicircular shoal which tended to focus waves on the flat behind the shoal. Many investigators have since performed computations over the same topography.

In these computations, regular waves were generated from one boundary using as input the time series of velocity from the fully nonlinear LPA wave forms. Odd derivatives of surface elevation were also specified at the boundary. On the transmitting boundary, a small amplitude boundary condition was combined with a zone where the evolution equations (6) and (7) gradually changed to become the advection equations

$$\frac{\partial}{\partial t}\left(\frac{\partial \eta}{\partial x}\right) = -c\frac{\partial}{\partial x}\left(\frac{\partial \eta}{\partial x}\right) \tag{14}$$

and

$$\frac{\partial}{\partial t}\left(\frac{\partial \phi_s}{\partial x}\right) = -c\frac{\partial}{\partial x}\left(\frac{\partial \phi_s}{\partial x}\right) \tag{15}$$

where c is some characteristic phase velocity on the shelf. These equations were solved in finite difference form using an upwinding scheme. This type of area around the boundary makes it very difficult for errors due to an imperfect boundary condition to propagate back into the domain, as they are continuously pushed out by the advection equations. All computations shown use the level of approximation $r = 3$.

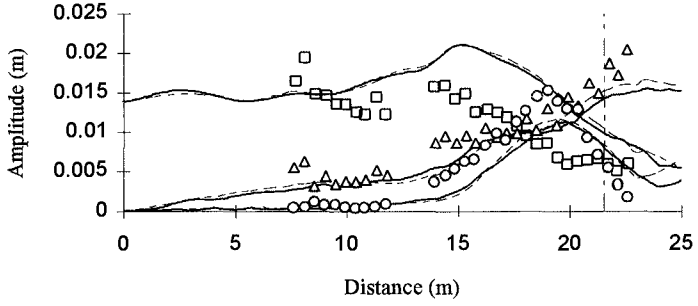

Figure 9(a). Harmonic Amplitudes along centreline of Whalin's topography, $T = 3$s, $A_1 = 0.0146$m. Solid lines indicate present results; dashed lines show results of Rygg (1988); symbols are experimental results of Whalin (1971). Chain-dashed line shows beginning of dissipating beach, which was not reproduced in computations.

Figure 9 shows the experimental and computational harmonic amplitudes along the centreline for the highest waves with experimental periods $T = 1$s, 2s, 3s. Also included are the results of Madsen and Sørensen (1992) using their extended Boussinesq equations for the $T = 1$s case and the results of Rygg (1988) using the Boussinesq equations of Peregrine (1967) for $T = 2$s, 3s.

For the longest wave, with $T = 3$s, both computational methods severely overpredict the amplitude of the first harmonic and moderately underpredict the amplitude of the second and third harmonics. Although the LPA results for $r = 3$ are shown, increasing the level to $r = 4$ (not shown here) provides no real change. This is somewhat distressing, as both LPA models and the extended Boussinesq equations should operate best in this range. However, the experimental topography used by Whalin was made up of a series of steps and only approximated the smooth topography used in the computations. Consequently, dissipation, neglected in computations, was significant in the experiments, especially for high, long waves. This is speculated to be the major source of discrepancies for this wave.

For the next wave, with $T = 2$s, computations agree somewhat better with experimental data. Once again, the first harmonic is overpredicted and so, to some degree, is the second harmonic, while the third harmonic is predicted relatively well. Both LPA and Bouusinesq computations predict similar features, although there are differences. One strange feature of this wave is that the initial amplitude of the first harmonic used to calculate the incoming waves, which is given as $A_1 = 0.0149$m, appears to be too high. In actual fact, it appears to be approximately $A_1 = 0.0135$m. Figure 9(c) shows LPA results for a wave with this initial amplitude, and agreement is much better. The final wave tested had a period of $T = 1$s, which gave it an initial length to depth ratio of $L/d = 3.27$. Of all waves, this was the best predicted. The computational values of the first harmonic are still slightly high on the final shoal but, aside from some numerical noise near the wave generator, the second harmonic is extremely well predicted. In contrast, the extended Boussinesq equations tend to somewhat underpredict the amplitude of the second harmonic.

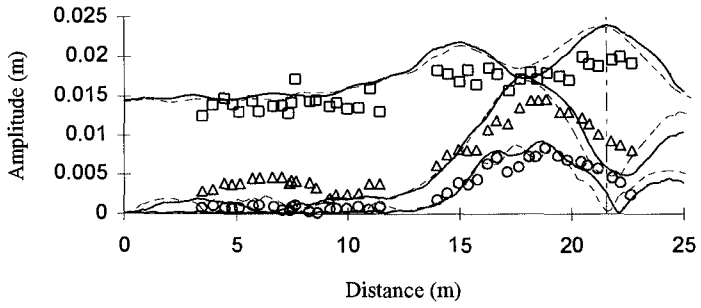

Figure 9(b). $T = 2$s, $A_1 = 0.0149$m. Dashed lines here are the Boussinesq results of Rygg (1988)

Overall, agreement between experiment and computations is not as good as would be hoped, possibly because of the neglect of dissipation in computations. It is worthwhile to note that for the cases $T = 2$s, 3s, where computations and experiments differed, both computational models behaved similarly. Therefore, it is believed that the dis-

crepancies result from something other than an inaccurate solution of the potential flow problem.

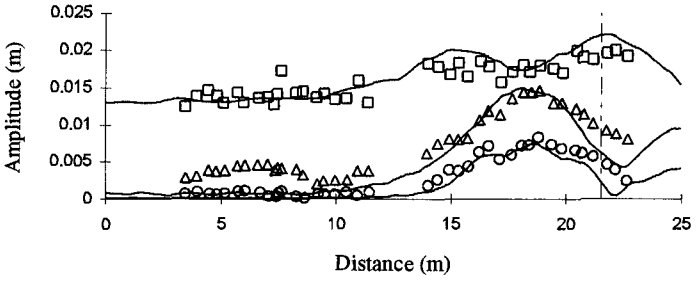

Figure 9(c). Experimental results from Whalin (1971) $T = 2$s, $A_1 = 0.0149$m. Computational results $T = 2$s, $A_1 = 0.0135$m.

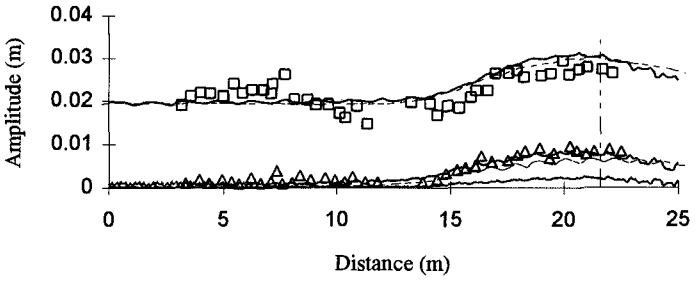

Figure 9(d). $T = 1$s, $A_1 = 0.0195$m. Dashed line shows extended Boussinesq results of Madsen and Sørensen (1992).

Conclusions

The local polynomial approximation method developed here has excellent linear and nonlinear properties for a wide range of waves. The simplicity of its formulation makes it an easy task to change the level of approximation, and thus the accuracy, of the method. Computations over varying topography show good accuracy for highly unsteady, nonlinear cases. For accurate potential flow computations in three dimensions, the LPA method is therefore an excellent choice for the numerical modeler.

References

Cokelet, E. D. (1977), Steep gravity waves in water of arbitrary uniform depth, *Phil. Trans Roy. Soc. London A* **286**, 183–230.

de Boor, C. (1978), *A practical guide to splines*. Springer-Verlag, New York, third edition.

de Haas, P., Dingemans, M., and Klopman, G. (1996), Simulation of free long-wave generation due to uneven bottoms, In *Proc. 25th Int. Conf. on Coastal Eng.*

Fenton, J. D. (1988), The numerical solution of steady water wave problems, *Computers and Geosciences* **14**, 357–368.

Fenton, J. D. and Kennedy, A. B. (1996), Fast methods for shoaling waves, In *Proc. 25th Int. Conf. Coastal Eng., Orlando.*

Gobbi, M. F. and Kirby, J. T. (1996), A fourth order fully nonlinear Boussinesq wave model, In *Proc. 25th Int. Conf. on Coastal Eng.*

Johnson, R. S. (1973), On the development of a solitary wave moving over an uneven bottom, *Proc. Camb. Phil. Soc.* **73**, 183–203.

Madsen, P. A. and Sørensen, O. R. (1992), A new form of the Boussinesq equations with improved linear dispersion characteristics. Part 2. A slowly-varying bathymetry, *Coastal Engng* **18**, 183–204.

Nwogu, O. (1993), An alternative form of the Boussinesq equations for nearshore wave propagation, *J. Waterway Port Coastal and Ocean Engng* **119**, 618–638.

Peregrine, D. (1967), Long waves on a beach, *J. Fluid Mech.* **27**(4), 815–827.

Rygg, O. B. (1988), Nonlinear refraction-diffraction of surface waves in intermediate and shallow depths, *Coastal Eng.* **12**, 191–211.

Schäffer, H. A. and Madsen, P. A. (1995), Further enhancements of Boussinesq-type equations, *Coastal Eng.* **26**, 1–14.

Shields, J. J. and Webster, W. C. (1988), On direct methods in water wave theory, *J. Fluid Mech.* **197**, 171–199.

Su, C. and Mirie, R. (1980), On head-on collisions between two solitary waves, *J. Fluid Mech.* **98**, 509–525.

Wang, P., Yao, Y., and Tulin, M. (1995), An efficient numerical tank for nonlinear water waves, based on the multi-subdomain approach with BEM, *Int. J. Numer. Meth. Fluids* **20**, 1315–1336.

Wei, G., Kirby, J., Grilli, S., and Subramanya, R. (1994), A fully nonlinear Boussinesq model for surface waves. 1. Highly nonlinear waves, Res. Rpt. CACR-94-15, Center for Applied Coastal Research, University of Delaware.

Witting, J. (1984), A unified model for the evolution of nonlinear water waves, *J. Comp. Phys* **56**, 203–236.